Boosting Reversibility and Stability of Zn Anodes via Manipulation of Electrolyte Structure and Interface with Addition of Trace Organic Molecules

Haiji Huang, Dongmei Xie, Jiachang Zhao, Pinhua Rao,* Won Mook Choi,* Kenneth Davey, and Jianfeng Mao*

The practical application of aqueous zinc-ion batteries (AZIBs) is significantly limited by poor reversibility and stability of the Zn anode. Here, the first time addition of trace organic gamma butyrolactone (GBL) is reported to a typical $ZnSO_4$ electrolyte to controllably manipulate the electrolyte structure and interface. Judiciously combined experimental characterization and theoretical computation confirm that the GBL additive weakens the bonding strength between Zn^{2+} ion and solvated H_2O and rearranges the "Zn^{2+}–H_2O–SO_4^{2-}-GBL" bonding network to reduce water activity and suppress corrosion and side products. The GBL molecules preferentially absorb on the surface of the Zn anode to give a uniform and compact Zn deposition. As a result, the Zn anode is boosted to run over 3105 cycles (6210 h) with average Coulombic efficiency of 99.93% under 1 mA cm^{-2} and 1 mAh cm^{-2}, and exhibit stable cycling for 1170 h under harsh testing conditions of 10 mA cm^{-2} and 10 mAh cm^{-2}. Additionally, the Zn–MnO$_2$ full cells using the ZnSO$_4$–GBL electrolyte exhibit a high capacity of 287 mAh g^{-1} at 0.5 A g^{-1} and good capacity retention of 87% following 400 cycles. These findings will be of immediate benefit to design low cost AZIBs for clean energy storage.

1. Introduction

To achieve carbon neutrality by 2050, a significantly increased use of clean energy technologies including, smart grid, electric vehicles (EVs) and energy efficient building retrofits, will be needed. Storage of energy is critical to underpinning sustainable consumer electronics, transport and industry smart grids. Li-ion batteries have been dominant. However, significant drawbacks include relative high cost and low safety.[1–3] Aqueous rechargeable zinc-ion batteries (AZIBs) have attracted research attention for large-scale energy storage because of advantageous, high safety, low toxicity, abundance of materials, and unique properties of zinc including, low redox potential (–0.7626 V vs standard hydrogen electrode), high gravimetric capacity (820 mAh g^{-1}), and high volumetric capacity (5585 mAh cm^{-3}).[4–7] Drawbacks however include, Zn dendrite formation, corrosion and by-product and H$_2$ evolution that mitigate against sufficiently high reversibility and stability.

Electrochemical behavior of Zn metal is determined principally by the properties of the aqueous electrolyte and electrode–electrolyte interface. These are closely related to the solvation structures of hydrated Zn^{2+} ions, anions, and hydrogen bonding network. Therefore, a reconstruction of the chemical bonding network and solvation structure of cations and anions in aqueous electrolyte, and optimization of the electrode–electrolyte interface can be used to practically regulate the performance of Zn anodes. Proposals to tune the solvation structure of electrolyte and boost reversibility of Zn anodes included, high concentration,[8–10] water-in-eutectic,[11–15] and aqueous/organic hybrid electrolytes.[16–19] Drawbacks from these electrolytes have included however, high cost, unwanted low ionic conductivity, and high viscosity. The addition of organics has been reported because these species, as liquids or solids can interact with Zn^{2+} and H$_2$O molecules to change the solvated structure of Zn hydration and the hydrogen bonding network without high concentration of slats or solvents.[20–30] However, the electrochemical performance of these Zn anodes remains poor, especially under harsh condition of high current density/capacity of up to 10 mA cm^{-2} and 10 mAh cm^{-2}. Additionally, particular organic molecules are highly flammable. Although

H. Huang, D. Xie, J. Zhao, P. Rao
College of Chemistry and Chemical Engineering
Shanghai University of Engineering Science
Shanghai 201620, P. R. China
E-mail: raopinhua@sues.edu.cn

H. Huang, W. M. Choi
School of Chemical Engineering
University of Ulsan
93 Daehak-ro Nam-gu, Ulsan 44610, Republic of Korea
E-mail: wmchoi98@ulsan.ac.kr

K. Davey, J. Mao
School of Chemical Engineering and Advanced Materials
The University of Adelaide
Adelaide, SA 5005, Australia
E-mail: jianfeng.mao@adelaide.edu.au

**ADVANCED
SCIENCE NEWS**

www.advancedsciencenews.com

**ADVANCED
ENERGY
MATERIALS**

www.advenergymat.de

the nonflammable nature of water assures safety of AZIBs, the hydrogen evolution reaction (HER) and/or oxygen evolution reaction (OER) during battery cycling and/or idling, lowers the Coulombic efficiency (CE) and cycle life and may cause explosions. Any application to AZIBs must therefore suppress these reactions without reducing practical safety. A nonflammable and/or low vapor pressure solvent is necessarily required therefore to regulate solvation structure and interface so as to boost reversibility and stability of Zn anodes under harsh conditions.

Because gamma-butyrolactone (GBL) has a high boiling and flash temperature, respectively, $T_b = 204$ °C and $T_f = 97$ °C, relatively low viscosity = 1.73 cP at 25 °C, good ionic conductivity, and a high dielectric constant $e = 39$, it is practically attractive as a solvent/additive for rechargeable batteries (Table S1, Supporting Information). GBL-based electrolytes have in fact been used in Li-ion batteries over a range of temperature.[31,32]

Here GBL was adopted as a new electrolyte additive to $ZnSO_4$ electrolyte. It was postulated that through adjusting volume percent of GBL in GBL-based electrolytes a small volume, ≈1% solvent, in 2 m $ZnSO_4$ would significantly boost Zn plating/stripping performance under different current density. Experiment and theoretical computation confirmed that the functional GBL additive weakens the bonding strength between Zn^{2+} ion and solvated H_2O and rearranges the "$Zn^{2+}–H_2O–SO_4^{2-}–GBL$" bonding network to reduce water activity and suppress corrosion and generation of by-product. The Zn metal surface absorbs GBL rather than H_2O which restricts uncontrollable 2D diffusion and gives rise to uniform deposition. Thus, the Zn–MnO_2 full cells using $ZnSO_4$-GBL electrolyte exhibited superior performance to that using GBL-free electrolyte. Importantly, because 2 m $ZnSO_4$-GBL electrolyte is nonflammable it makes AZIBs practically promising for large-scale application.

2. Results and Discussion

The stability of the Zn electrode in aqueous electrolyte with and without GBL was compared in Zn‖Zn symmetric cells, **Figure 1**a–c (Figures S1–S3, Supporting Information). GBL addition resulted in excellent stability of Zn in Zn‖Zn in normal to harsh condition. With an optimized electrolyte of 2 m $Zn(SO_4)_2$ with 1% GBL in volume (2MG1), the Zn symmetrical cell exhibited highly stable cycling performance for over 4200 h at a current density of 1 mA cm^{-2} and an areal capacity of 1 mAh cm^{-2}, significantly however, the 2 m $ZnSO_4$ electrolyte failed following 700 h, Figure 1a. Under harsh conditions of 10 mA cm^{-2} and 10 mAh cm^{-2}, the Zn electrode with 2MG1 electrolyte remained stable and exhibited reversible Zn plating/stripping for 1170 h. Importantly, this is significantly longer than that in the blank electrolyte of 70 h, Figure 1b. At a high 20 mA cm^{-2} and 20 mAh cm^{-2}, Figure 1c, the Zn electrode in the symmetrical cell with optimized electrolyte exhibited stable cycling for >140 h, while the Zn electrode in the blank electrolyte exhibited a short circuit in <25 h. These findings strongly evidence the significant boost in reversibility and stability of the Zn anodes resulting from GBL addition. To confirm the highly significant impact of GBL addition, the cumulative plated capacity (CPC) was compared directly with selected, representative published data, Figure 1d (Table S2,S3, Supporting Information). Significantly, it is seen in the figure (and table)

that the ultrahigh CPC of 5.85 Ah cm^{-2} exhibited at current density 10 mA cm^{-2} for the $ZnSO_4$-GBL electrolyte exceeds that for many published electrolyte additives.

Reversibility of the Zn electrode in aqueous electrolyte with and without GBL was compared in Zn‖Cu asymmetric cells, **Figure 2**a–d (Figures S4 and S5, Supporting Information). It was found that there are marginal differences in the initial Coulombic efficiency, that increases with increasing $ZnSO_4$ concentration, i.e., 2MG1 > 2 m > 1MG1 > 0.5MG1 > 0.25MG1 (Figure S4, Supporting Information). The addition of less or more GBL, reduced the initial Coulombic efficiency (Figure S5, Supporting Information). The presence of 1% GBL boosted the initial Coulombic efficiency to 92.1% at 1 mA cm^{-2} and 1 mAh cm^{-2}, and the average CE increased to 99.93% for over 3105 cycles (6210 h), Figure 2a. In comparison, the 2 m $ZnSO_4$ electrolyte exhibited a low initial Coulombic efficiency of 91.7% and an average CE of 99.6%, noticeably failing at the 222th cycle, Figure 2a,b. As is shown in Figure 2c,d, the addition of GBL increased the overpotential for Zn plating/stripping on the Cu surface at the first cycle, but reduced it following cycling; a finding due to increased, or reduced interphasic resistance as compared with blank electrolyte (Figure S6, Supporting Information).

Addition of GBL concomitantly tuned Zn deposition morphology and suppressed corrosion. The scanning electron microscopy (SEM) images) confirmed that following 50 cycles with Zn‖Cu cells, the Zn surface in the $ZnSO_4$ electrolyte become an apparent scattered microporous structure, Figure 2e, while there remained a large-area connected vertical arrangement of sheet structure on the Zn surface in the $ZnSO_4$-GBL electrolyte; this formed a densely integrated binding network, Figure 2f. XRD findings for the Zn electrode following cycling showed $Zn((OH)_2)_3(ZnSO_4)H_2O)_5$ by-product in the $ZnSO_4$ electrolyte. The peaks however for $Zn((OH)_2)_3(ZnSO_4)H_2O)_5$ were significantly reduced in $ZnSO_4$-GBL electrolyte, confirming that Zn electrode corrosion was significantly suppressed, Figure 2g. The morphology and structure of Zn at higher current density and areal capacity (10 mA cm^{-2}, 10 mAh cm^{-2}) also suggested that 2MG1 electrolyte enables the smooth and compact surface and less by-products, which further confirms the effeteness of GBL to regulate the Zn deposition and suppress the corrosion (Figures S7 and S8, Supporting Information). These findings were confirmed via a linear polarization test. As is seen in **Figure 3**a, the Zn electrode in $ZnSO_4$-GBL electrolyte exhibited a greater corrosion voltage of −0.933 V compared with that for pure $ZnSO_4$ electrolyte of − 0.922 V. This finding evidences a lowered tendency for corrosion side reactions in $ZnSO_4$-GBL electrolyte. A reduced hydrogen and oxygen evolution current obtained from linear sweep voltammetry (LSV) curves confirms the impact on boosting reversibility and stability via controlled manipulation with GBL additive (Figure S9, Supporting Information). The Zn anodes showed the electric double-layer capacitance (EDLC) values of 62.36 and 54.6 µF cm^{-2} in 2 m $ZnSO_4$ with no additive and with GBL additive, respectively (Figure S10, Supporting Information). The slightly lower EDLC in GBL-added electrolyte indicates that the GBL could be an appropriate additive, which favors the diffusion of Zn^{2+} without sacrificing the reaction kinetics of Zn anodes. The contact angle of the Zn electrode in $ZnSO_4$-GBL was determined as 64.0°, less than that in $ZnSO_4$
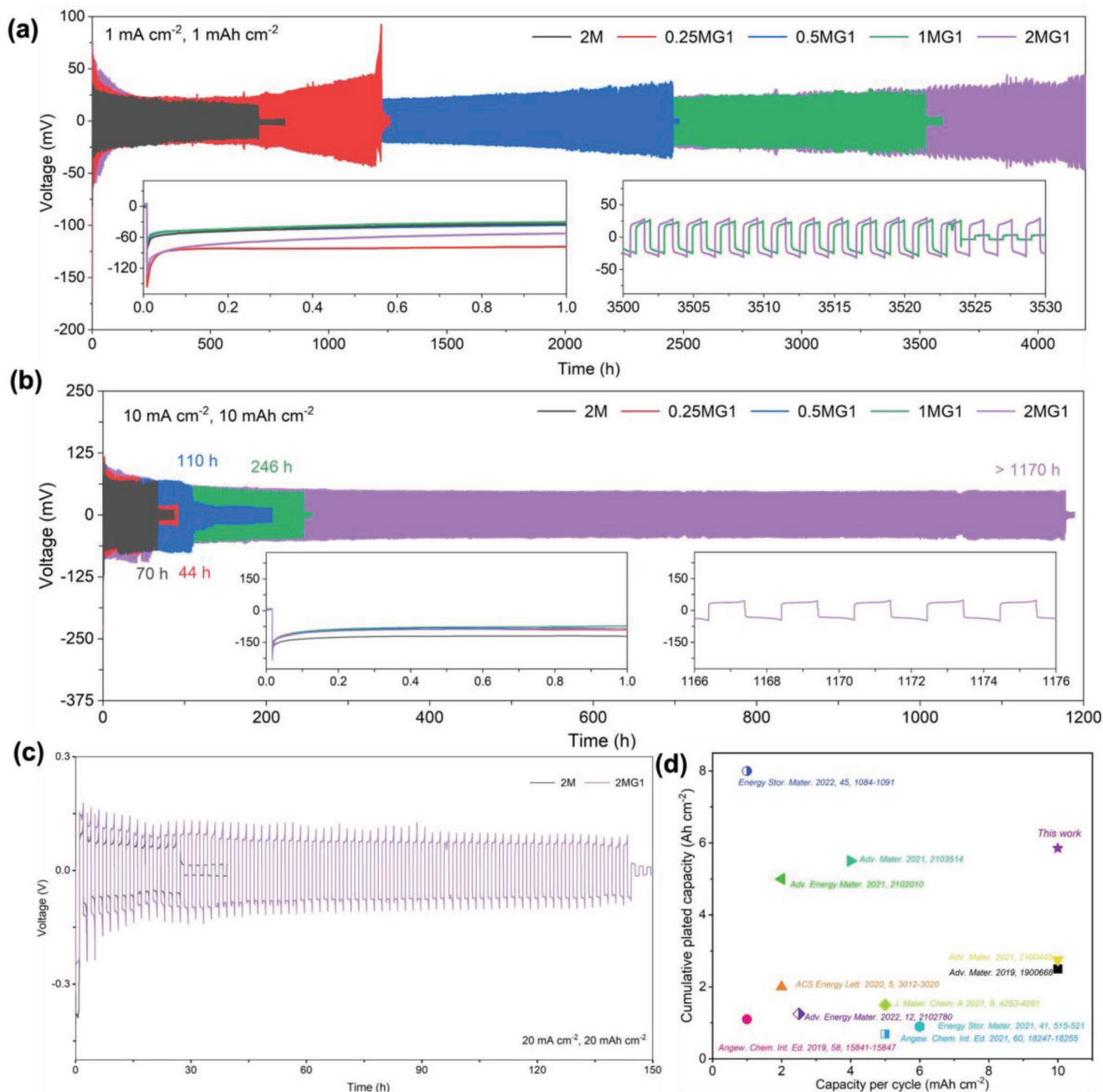
Figure 1. Zn∥Zn plating/stripping and stability. Zn∥Zn symmetric cells containing differing concentration of ZnSO$_4$ with same volume percent of additive at current density and areal capacity of a) 1 mA cm^{-2} at 1 mAh cm^{-2}, b) 10 mA cm^{-2} at 10 mAh cm^{-2} and c) 20 mA cm^{-2} at 20 mAh cm^{-2}. d) Cumulative plated capacity versus capacity per cycle of 2MG1 electrolyte compared with selected others.

of 75.0°, Figure 3b. This difference aids practically in a uniform electric distribution and production of homogeneous plating of Zn. Furthermore, in situ optical microscopy was employed to monitor the surface morphology evolution during the Zn plating process. Clearly, there are many Zn protrusions formed on the surface in ZnSO$_4$ electrolytes (2 M) (Figure S11a, Supporting Information), while the surface almost changes little in the GBL added electrolytes (2MG1) (Figure S11b, Supporting Information). The results further demonstrate the dendrite inhibitor of adsorbed GBL. The

uniform deposition and suppressed corrosion result in high reversibility and stability of Zn chemistry.

Judiciously combined experimental characterizations including, nuclear magnetic resonance (NMR), Fourier transform infrared spectroscopy (FTIR) and Raman spectra, together with theoretical computations were used to determine the underlying mechanism for Zn metal in ZnSO$_4$-GBL. ^{2}H NMR spectra showed that the ^{2}H peak in the electrolyte shifted from 4.683 to 4.697 ppm following addition of GBL, Figure 3c, evidencing a decreased surrounding electronic density and
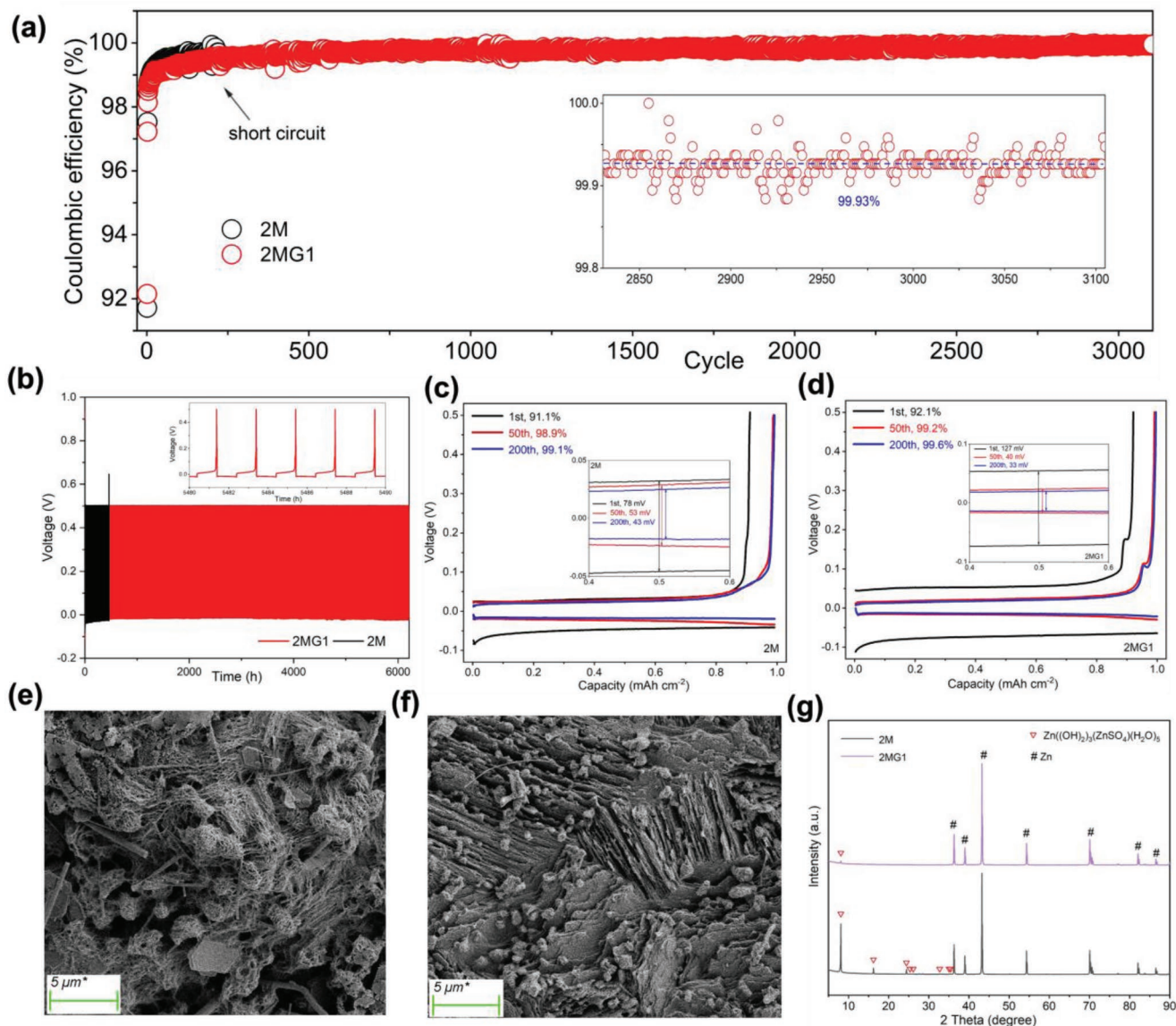
Figure 2. Zn||Cu half cell performance and properties. a) Coulombic efficiency (CE) for cells in 2 M ZnSO$_4$ electrolyte with (2MG1) and without (2 M) 1% GBL. b) Time–voltage curves. Charge/discharge voltage profiles of half cell with c) 2 M and d) 2MG1 electrolyte at 1st, 50th and 200th cycle with magnified view of corresponding cycles in capacity range between 0.4 and 0.6 mAh cm^{-2} at current density 1 mA cm^{-2}. SEM images of Zn-foil in e) 2 M and f) 2MG1 electrolyte for half cells following 50 cycles. g) XRD spectra for Zn-foil in 2 M and 2MG1 electrolyte for half cells following 50 cycles.

a weakened shielding of protons in water because of interaction between GBL and D$_2$O. The addition of GBL weakens the solvation coordination between Zn^{2+} and water. This finding was confirmed via FTIR and Raman results. Compared with pure GBL, the C−H stretching moves to lower wave number in ZnSO$_4$-GBL caused by interaction between GBL and water, Figure 3d. The strong interaction between GBL and H$_2$O without interference of Zn^{2+} was evidenced via findings from FTIR, Figure 3d (Figure S12, Supporting Information). It can be seen in the figure that compared with ZnSO$_4$ electrolyte, the ν (SO$_4^{2-}$) vibration is shifted in ZnSO$_4$-GBL, Figure 3e. This shift vibration is evidenced in the Raman spectra, Figure 3f, and is attributed to the impaired electrostatic coupling between Zn^{2+} and SO$_4^{2-}$ because of the presence of GBL.

Molecular dynamics (MD) simulation was used to analyze the electrolyte structure of pure ZnSO$_4$ and ZnSO$_4$-GBL. In Zn aqueous electrolyte, Zn^{2+} is typically coordinated by 4–6 H$_2$O molecules, whereas SO$_4^{2-}$ anions mainly coordinate with hydrated Zn^{2+} through the hydrogen bonding-network formed by H$_2$O molecules (Figure S13, Supporting Information). There are additional interactions amongst GBL, Zn^{2+}, SO$_4^2$ and H$_2$O that are present in the ZnSO$_4$-GBL electrolyte, Figure 3g. Corresponding radial distribution functions (RDFs) and average coordination number (ACN) were obtained, Figure 3h (Figure S14, Supporting Information). With the addition of GBL, the peak for Zn−O pair in the RDF curve shifted from 1.95 to 1.85 Å, evidencing that GBL has a significant impact on constraining water. The average coordination number for Zn-H$_2$O
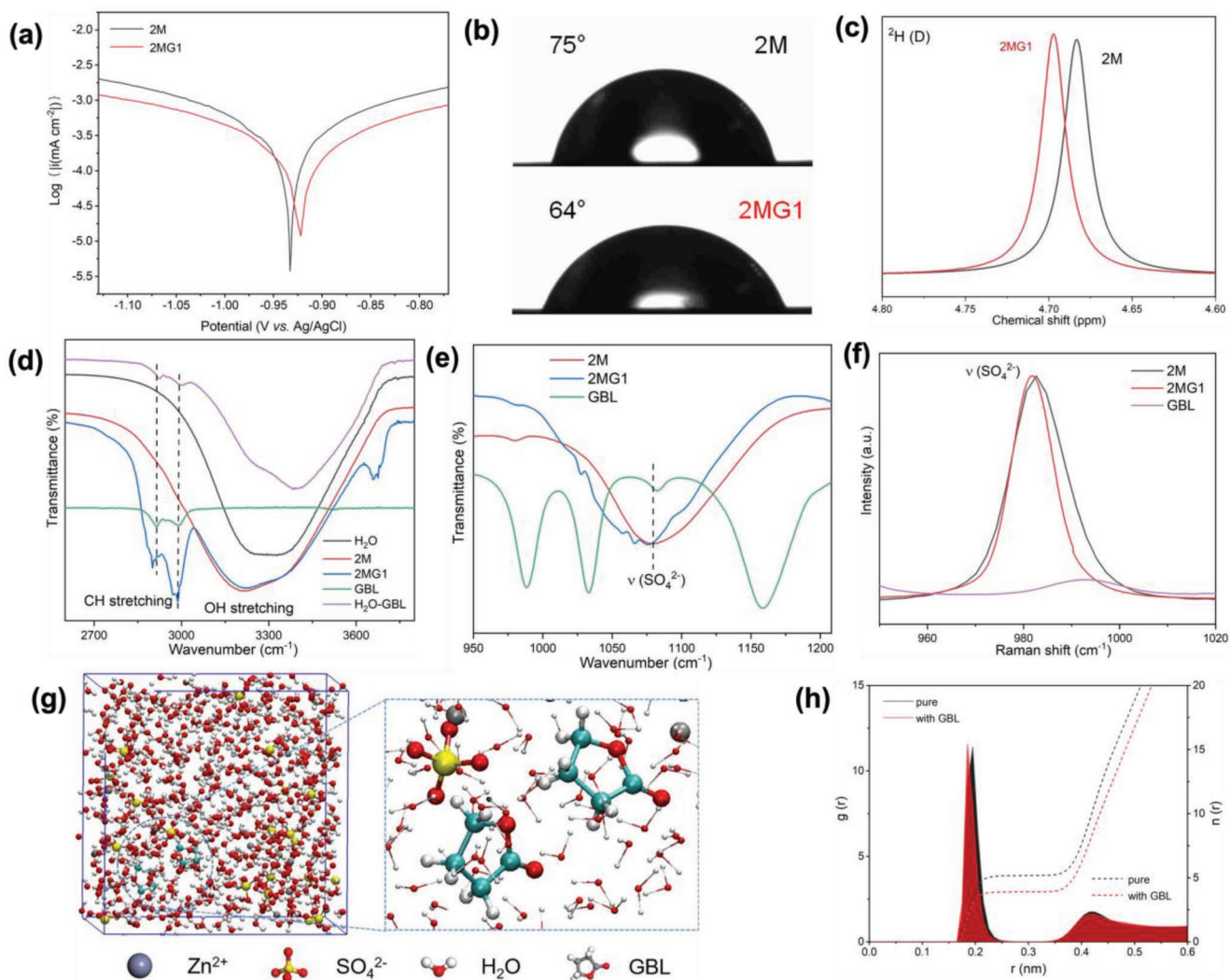
2202419 (4 of 9)

Figure 3. Chemical and physical properties of electrolytes. a) Polarization of corrosion curve, b) Contact angle measurement of electrolytes with Zn-foil and c) ^{2}H NMR spectra for 2 M and 2MG1 electrolyte. FT-IR spectra for H_2O, H_2O-GBL, GBL, 2 M and 2MG1. d) CH- and OH-stretching, e) $v(SO_4^{2-})$. f) Raman spectra for 2 M, 2MG1 and GBL. g) 3D snapshot with enlarged area of ZnSO$_4$-GBL and h) RDF and coordination number for Zn^{2+}-O (H_2O) from MD simulations.

in the first hydration layer was reduced from 5.2 in ZnSO$_4$ to 3.9 for ZnSO$_4$-GBL as shown by short dashed line in Figure 3h, confirming that the interaction of GBL and H_2O weakened the preferred coordination between Zn^{2+} and H_2O was in aqueous electrolyte. Combined, the experimental findings from NMR, FTIR and Raman, together with those from MD simulations, confirm that the GBL additive tunes the electrolyte structure by rearranging the "Zn^{2+}-H_2O-SO_4^{2-}-GBL" bonding network as a result of the additional interactions amongst GBL, anions, and cations in ZnSO$_4$ aqueous electrolyte, with GBL additive.

The interaction amongst Zn^{2+} ion, H_2O, and GBL molecules was assessed via quantum chemistry computation. Based on the binding energy results of **Figure 4**a, GBL molecules are more preferred to Zn ions than H_2O. The binding energies of both Zn^{2+}-GBL and Zn^{2+}-H_2O are greater than for GBL-H_2O. This finding is consistent with that for the electrolyte structure simulated by MD. Figure 4b highlights that following replacing one H_2O molecule with one GBL molecule in the primary solvation shell

of Zn^{2+}-H_2O, the regional value of the partial electrostatic potential (ESP) decreases. This evidences that electrostatic repulsion around Zn^{2+} is impacted to give rapid transmission. This finding agreed with that from mean-squared displacement versus time where the diffusion coefficient for Zn^{2+} was increased following addition of GBL (Figure S15, Supporting Information).

The adsorption ability between Zn slab and GBL or H_2O in ZnSO$_4$-GBL electrolyte was studied and compared via ab initio computation. The adsorption of H_2O on the Zn slab ((002) or (101) crystal plane) at possible sites was found to be relatively weak as is shown in Figure 4c (Figure S16, Supporting Information). There exists therefore stronger interplay between Zn and GBL on a parallel position along the Zn surface (GBL (P)). These findings confirm that the GLB molecules are absorbed on the surface of Zn so as to be parallel and to inhibit uncontrolled 2D diffusion and facilitate uniform and compact Zn deposition as was seen in the SEM images. Following addition of GBL the nucleation overpotential increased from 130.86 to
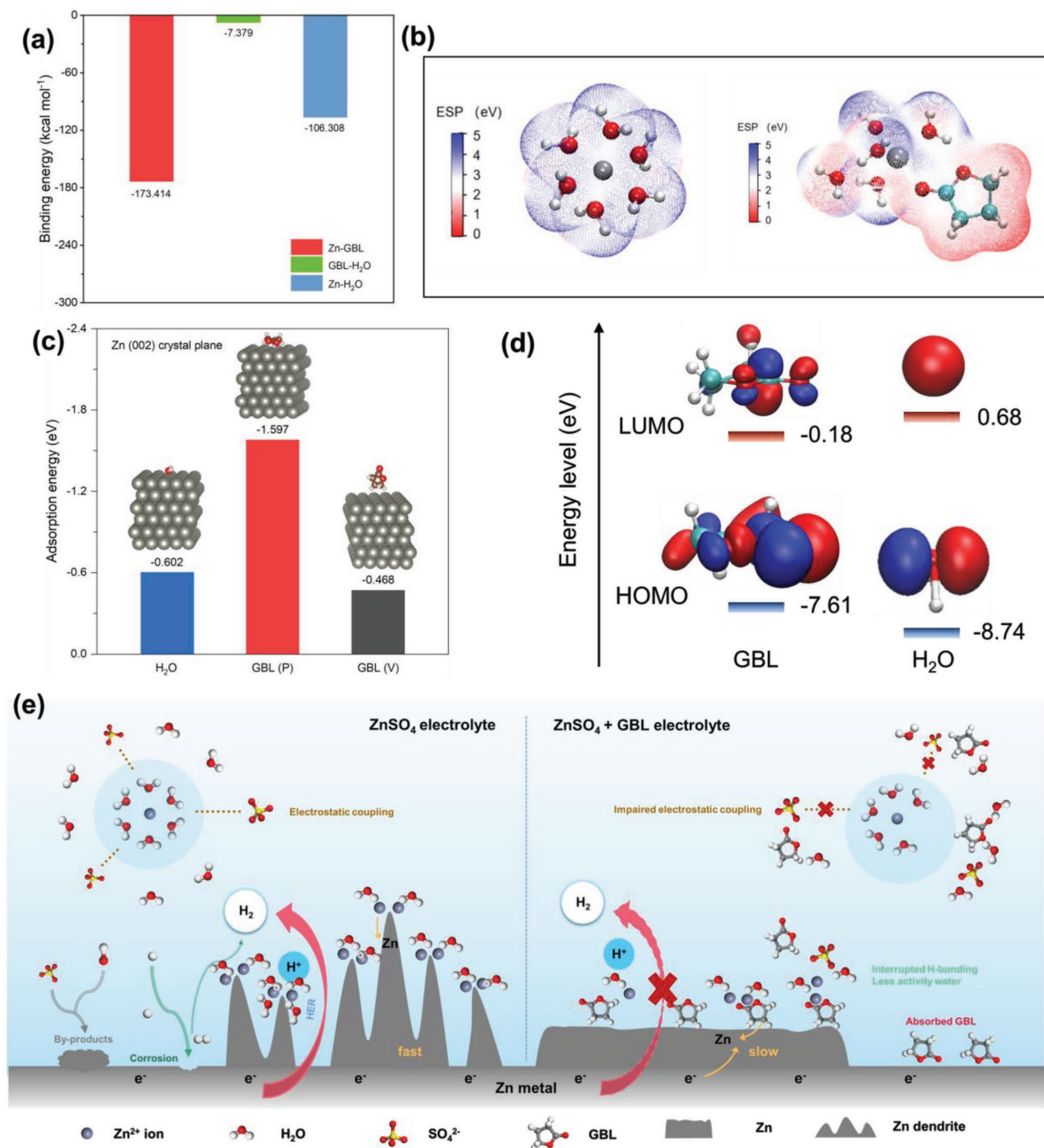
2202419 (5 of 9)

Figure 4. Theoretical computations and schematic for ZnSO₄-GBL electrolyte. a) Binding energy for Zn^{2+} with differing compounds from DFT computation. b) Electrostatic potential mapping of original Zn^{2+}-6H₂O (Left) and Zn^{2+}-5H₂O-GB (Right) solvation structures. c) Comparison of adsorption energy of H_2O and GBL molecules on Zn (002) crystal plane. Inset shows corresponding absorbed model. d) LUMO and HOMO iso-surface (iso-value = 0.02 a.u.) of H_2O (Right) and GBL (Left) molecules. e) Schematic for mechanism for ZnSO₄ and ZnSO₄-GBL electrolyte.

165.03 mV (Figure S17, Supporting Information), underscoring a slow zinc deposition. The Nyquist plots confirm that there is greater charge transfer resistance, Figure S6a (Supporting Information), as is in agreement with the findings from theoretical computation. Electron gain and loss of absorbed molecules

on the Zn surface will impact the deposition behavior of zinc. As is seen in Figure 4d, because GBL has a greater highest occupied molecular orbital (HOMO) than that for H_2O, respectively, – 7.61 versus – 8.74 eV, electrons in GBL are more readily lost when absorbing on the Zn surface. It is apparent
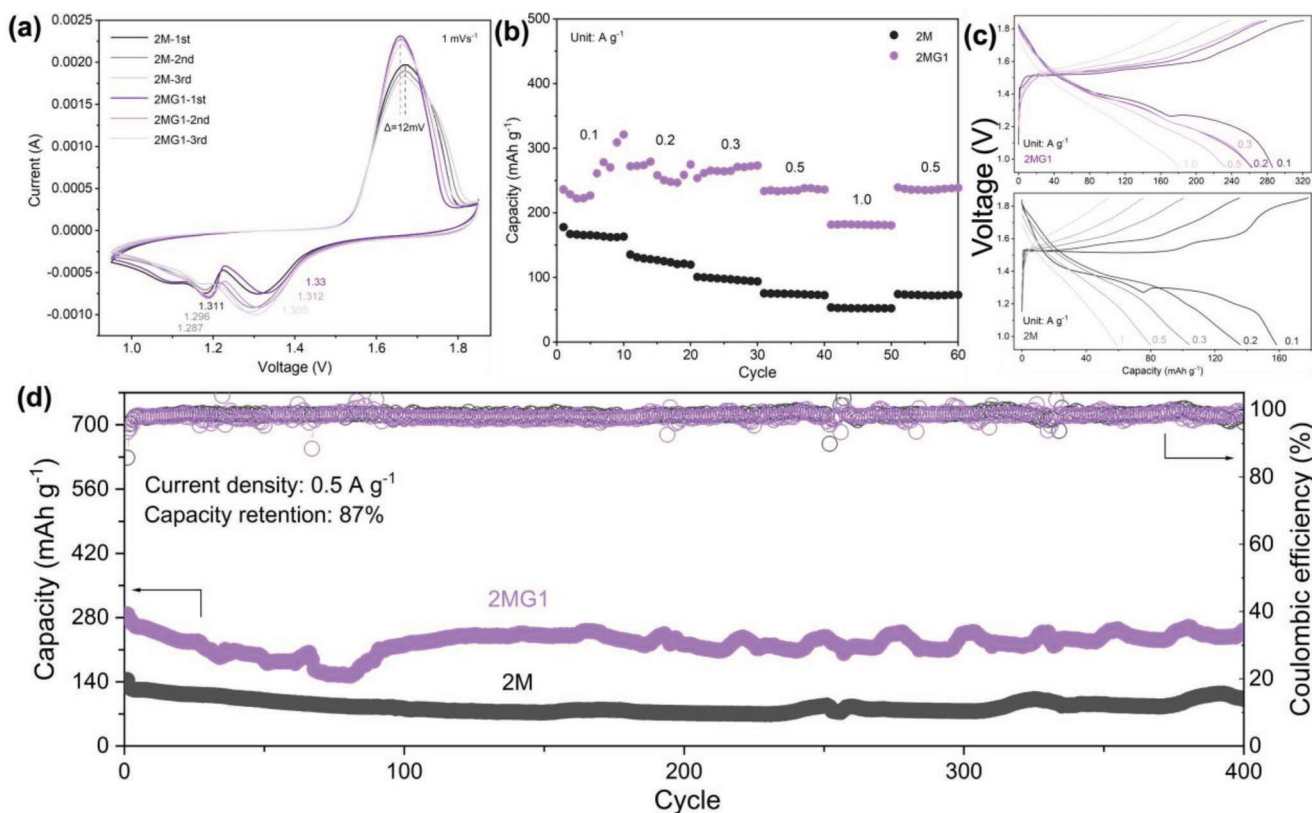
**ADVANCED
SCIENCE NEWS**

www.advancedsciencenews.com

**ADVANCED
ENERGY
MATERIALS**

www.advenergymat.de

Figure 5. Zn||MnO$_2$ full cell performance. a) Cyclic voltammetry curves for 1st, 2nd and 3rd cycle. b) Rate capability at 0.1, 0.2, 0.3, 0.5, and 1 A g^{-1} and back to 0.5 A g^{-1}. c) Galvanostatic charge and discharge (GCD) profiles at current density of 0.1, 0.2, 0.3, 0.5 and 1 A g^{-1} and d) Cycle performance of full cell with 2 M and 2MG1 electrolyte.

from the 3D iso-surface models (Figure S18, Supporting Information for ZSC-002 and Figure S19, Supporting Information for ZSC-101), together with corresponding 2D contours (Figure S20, Supporting Information for ZSC-002 and Figure S21, Supporting Information for ZSC-101), that electrons transfer from GBL to Zn via adsorption, therefore confirming strong chemical adsorption of GBL.

The overall mechanism postulated for boosted Zn anodes via addition of GBL is given in Figure 4e. During Zn deposition, the hydrated $[Zn(H_2O)_n]^{2+}$ in pure ZnSO$_4$ electrolyte brings significant numbers of H$_2$O molecules that are reduced to release H$_2$. The increase in local pH because of H$_2$ evolution promotes formation of Zn^{2+}-insulating hydroxide zinc–salt passivation on the Zn surface and reduces Zn utilization and cycle life, and promotes Zn dendrite growth. In comparison with addition of GBL, the average coordination number of Zn–H$_2$O in the primary hydration layer is reduced, and the bonding strength between Zn^{2+} ion and solvated H$_2$O is weakened. This additional interaction amongst GBL, Zn^{2+}, SO$_4^{2-}$, and H$_2$O rearranges the "Zn^{2+}–H$_2$O–SO$_4^{2-}$–GBL" bonding network, reduces water activity and generation of by-product $(Zn(OH)_2)_3(ZnSO_4)(H_2O)_3$. Moreover, GBL molecules absorb on the Zn surface, regulating the homogeneous distribution of Zn^{2+} flux and restricting uncontrolled 2D diffusion that results in uniform and compact Zn deposition. Because of function in both electrolyte structure, and at the electrode–electrolyte interface, the GBL additive boosts the reversibility and cycling stability

of Zn anodes. Importantly, because ZnSO$_4$-GBL electrolyte is nonflammable (Figure S22, Supporting Information), it is practically attractive for large-scale applications. Its high boiling and flash point contribute to safety and reduced risk of explosion including, in electrolyte leakage and thermal runaway.

To assess the practical feasibility of GBL addition in boosting performance of the full cells, Zn–MnO$_2$ full cells were assembled in which the MnO$_2$ was synthesized with β phase and nanorod morphology (Figures S23 and S24, Supporting Information).[25] With limited GBL addition, the performance of Zn–MnO$_2$ cells was boosted as was confirmed in cyclic voltammetry (CV), rate performance from 0.1 to 1 A g^{-1} and galvanostatic charge–discharge (GCD), **Figure 5**a–c. The Zn–MnO$_2$ full cells using ZnSO$_4$-GBL electrolyte exhibited a high capacity of 287 mAh g^{-1} at 0.5 A g^{-1} and good capacity retention of 87% following 400 cycles, Figure 5d. Moreover, the Zn–MnO$_2$ full cells using ZnSO$_4$-GBL electrolyte deliver higher capacity and superior stability than that using pristine ZnSO$_4$ electrolyte at high current density of 5 A g^{-1} (Figure S25, Supporting Information). Ex situ XRD measurements suggest both Zn^{2+} intercalation and H$^+$ conversion reactions in MnO$_2$ at both electrolytes (Figure S26, Supporting Information). Kinetic analysis indicates that the electrochemical charge storage in MnO$_2$ cathode in both electrolytes is contributed by both nondiffusion controlled and solid-state ion diffusion controlled reactions (Figure S27, Supporting Information), while 2MG1 electrolyte enables larger capacitive contribution.[33,34]

The 2MG1 electrolyte also enables higher diffusion coefficient for the MnO_2 structure during the intercalation process than that at 2 M. This is mainly associated with the electrolyte media for redox reactions where the addition of GBL reshapes the solvation structure, facilitating the charge transport (Figure S28, Supporting Information). MnO_2 electrode in GBL-added electrolyte also shows lower charge-transfer resistance (Figure S29, Supporting Information) and better wettability (Figure S30, Supporting Information) than that in pristine $ZnSO_4$ electrolyte, which would further benefit the capability of MnO_2 cathode. Significantly, the cathode following 50 cycles was retained as the fresh electrode, confirming the stability of MnO_2 in the $ZnSO_4$-GBL electrolyte (Figure S31, Supporting Information).

3. Conclusion

Trace low vapor pressure organic solvent, gamma butyrolactone (GBL) can be used to controllably manipulate typical $ZnSO_4$ electrolyte to give a highly stable and reversible aqueous zinc-ion battery (AZIB). Combined experiment, including, NMR, FTIR, and Raman analysis, together with theoretical computation using MD and DFT confirmed that functional GBL manipulates the electrolyte structure by rearranging the "Zn^{2+}–H_2O–SO_4^{2-}–GBL" bonding network and altering Zn anode–electrolyte interface via absorption of GBL on the Zn surface. This reduces the water activity, suppresses corrosion and generation of by-product, and gives a uniform compact Zn deposition. The anode ran over 3105 cycles (6210 h) with an average CE of 99.93% under 1 mA cm^{-2} and 1 mAh cm^{-2}, and; exhibited stable and reversible Zn plating/stripping cycling for 1170 h under testing conditions of 10 mA cm^{-2} and 10 mAh cm^{-2}. The reversibility and stability of the Zn anode significantly outperformed that using $ZnSO_4$ electrolyte. The Zn–MnO_2 full cells using $ZnSO_4$-GBL electrolyte exhibited a high capacity of 287 mAh g^{-1} at 0.5 A g^{-1} and an improved cycling stability (87% capacity retention following 400 cycles). These findings offer a quantitative engineering strategy to boost reversibility and stability of Zn anodes in rechargeable AZIBs. Importantly, because the 2 M $ZnSO_4$-GBL electrolyte is nonflammable, it makes AZIBs advantageous for large-scale and low-cost application in electrical-grid storage and clean energy storage.

Supporting Information

Supporting Information is available from the Wiley Online Library or from the author.

Acknowledgements

Conflict of Interest

The authors declare no conflict of interest.

Data Availability Statement

The data that support the findings of this study are available from the corresponding author upon reasonable request.

Keywords

[1] M. Li, J. Lu, Z. Chen, K. Amine, *Adv. Mater.* **2018**, *30*, 1800561.
[2] J. Wu, Y. Cao, H. Zhao, J. Mao, Z. Guo, *Carbon Energy* **2019**, *1*, 57.
[3] J. Mao, C. Ye, S. Zhang, F. Xie, K. Davey, R. Zeng, Z. Guo, S. Qiao, *Energy Environ. Sci.* **2022**, *15*, 2732.
[4] M. Song, H. Tan, D. Chao, H. J. Fan, *Adv. Funct. Mater.* **2018**, *28*, 1802564.
[5] T. Zhang, Y. Tang, S. Guo, X. Cao, A. Pan, G. Fang, J. Zhou, S. Liang, *Energy Environ. Sci.* **2020**, *13*, 4625.
[6] S. L. Liu, R. Z. Zhang, J. F. Mao, Y. L. Zhao, Q. Cai, Z. P. Guo, *Sci. Adv.* **2022**, *8*, eabn5097.
[7] Y. Wang, Z. Wang, F. Yang, S. Liu, S. Zhang, J. Mao, Z. Guo, *Small* **2022**, https://doi.org/10.1002/smll.202107033.
[8] F. Wang, O. Borodin, T. Gao, X. Fan, W. Sun, F. Han, A. Faraone, J. A. Dura, K. Xu, C. Wang, *Nat. Mater.* **2018**, *17*, 543.
[9] C. Zhang, J. Holoubek, X. Wu, A. Daniyar, L. Zhu, C. Chen, D. P. Leonard, I. A. Rodríguez-Pérez, J.-X. Jiang, C. Fang, X. Ji, *Chem. Commun.* **2018**, *54*, 14097.
[10] Y. Zhu, J. Yin, X. Zheng, A.-H. Emwas, Y. Lei, O. F. Mohammed, Y. Cui, H. N. Alshareef, *Energy Environ. Sci.* **2021**, *14*, 4463.
[11] J. Zhao, J. Zhang, W. Yang, B. Chen, Z. Zhao, H. Qiu, S. Dong, X. Zhou, G. Cui, L. Chen, *Nano Energy* **2019**, *57*, 625.
[12] W. Yang, X. Du, J. Zhao, Z. Chen, J. Li, J. Xie, Y. Zhang, Z. Cui, Q. Kong, Z. Zhao, C. Wang, Q. Zhang, G. Cui, *Joule* **2020**, *4*, 1557.
[13] J. Shi, T. Sun, J. Bao, S. Zheng, H. Du, L. Li, X. Yuan, T. Ma, Z. Tao, *Adv. Funct. Mater.* **2021**, *31*, 2102035.
[14] X. Lin, G. Zhou, M. J. Robson, J. Yu, S. C. T. Kwok, F. Ciucci, *Adv. Funct. Mater.* **2022**, *32*, 2109322.
[15] D. Han, C. Cui, K. Zhang, Z. Wang, J. Gao, Y. Guo, Z. Zhang, S. Wu, L. Yin, Z. Weng, F. Kang, Q.-H. Yang, *Nat. Sustainability* **2022**, *5*, 205.
[16] S. Liu, J. Mao, W. K. Pang, J. Vongsvivut, X. Zeng, L. Thomsen, Y. Wang, J. Liu, D. Li, Z. Guo, *Adv. Funct. Mater.* **2021**, *31*, 2104281.
[17] J. Hao, L. Yuan, C. Ye, D. Chao, K. Davey, Z. Guo, S.-Z. Qiao, *Angew. Chem., Int. Ed.* **2021**, *60*, 7366.
[18] N. Chang, T. Li, R. Li, S. Wang, Y. Yin, H. Zhang, X. Li, *Energy Environ. Sci.* **2020**, *13*, 3527.
[19] J. Q. Huang, X. Y. Guo, X. Y. Lin, Y. Zhu, B. Zhang, *Research* **2019**, *2019*, 10.
[20] D. Wang, Q. Li, Y. Zhao, H. Hong, H. Li, Z. Huang, G. Liang, Q. Yang, C. Zhi, *Adv. Energy Mater.* **2022**, *12*, 2102707.
[21] H. Lu, X. Zhang, M. Luo, K. Cao, Y. Lu, B. B. Xu, H. Pan, K. Tao, Y. Jiang, *Adv. Funct. Mater.* **2021**, *31*, 2103514.
[22] J. Cui, X. Liu, Y. Xie, K. Wu, Y. Wang, Y. Liu, J. Zhang, J. Yi, Y. Xia, *Mater. Today Energy* **2020**, *18*, 100563.

[23] L. Cao, D. Li, E. Hu, J. Xu, T. Deng, L. Ma, Y. Wang, X.-Q. Yang, C. Wang, *J. Am. Chem. Soc.* **2020**, *142*, 21404.

[24] P. Sun, L. Ma, W. Zhou, M. Qiu, Z. Wang, D. Chao, W. Mai, *Angew. Chem., Int. Ed.* **2021**, *60*, 18247.

[25] L. Cao, D. Li, T. Pollard, T. Deng, B. Zhang, C. Yang, L. Chen, J. Vatamanu, E. Hu, M. J. Hourwitz, L. Ma, M. Ding, Q. Li, S. Hou, K. Gaskell, J. T. Fourkas, X.-Q. Yang, K. Xu, O. Borodin, C. Wang, *Nat. Nanotechnol.* **2021**, *16*, 902.

[26] L. Ma, T. P. Pollard, Y. Zhang, M. A. Schroeder, M. S. Ding, A. V. Cresce, R. Sun, D. R. Baker, B. A. Helms, E. J. Maginn, C. Wang, O. Borodin, K. Xu, *Angew. Chem., Int. Ed.* **2021**, *60*, 12438.

[27] Q. Zhang, J. Luan, L. Fu, S. Wu, Y. Tang, X. Ji, H. Wang, *Angew. Chem., Int. Ed.* **2019**, *58*, 15841.

[28] C. Huang, X. Zhao, S. Liu, Y. Hao, Q. Tang, A. Hu, Z. Liu, X. Chen, *Adv. Mater.* **2021**, *33*, 2100445.

[29] M. D. Yan, N. Dong, X. S. Zhao, Y. Sun, H. L. Pan, *ACS Energy Lett.* **2021**, *6*, 3236.

[30] X. Zeng, K. Xie, S. Liu, S. Zhang, J. Hao, J. Liu, W. K. Pang, J. Liu, P. Rao, Q. Wang, J. Mao, Z. Guo, *Energy Environ. Sci.* **2021**, *14*, 5947.

[31] D. Belov, D. T. Shieh, *J. Solid State Electrochem.* **2012**, *16*, 603.

[32] T. Doi, Y. Shimizu, M. Hashinokuchi, M. Inaba, *ChemElectroChem* **2017**, *4*, 2398.

[33] Y. Jin, L. Zou, L. Liu, M. H. Engelhard, R. L. Patel, Z. Nie, K. S. Han, Y. Shao, C. Wang, J. Zhu, H. Pan, J. Liu, *Adv. Mater.* **2019**, *31*, 1900567.

[34] Q. Tan, X. Li, B. Zhang, X. Chen, Y. Tian, H. Wan, L. Zhang, L. Miao, C. Wang, Y. Gan, J. Jiang, Y. Wang, H. Wang, *Adv. Energy Mater.* **2020**, *10*, 2001050.

2202419 (9 of 9)